Inter-residue Coupling and Equilibrium Unfolding of PPII Helical Peptides. Vibrational Spectra Enhanced with ^{13}C Isotopic Labeling

Heng Chi, Ahmed Lakhani, Anjan Roy, Marcelo Nakaema, and Timothy A. Keiderling*

Department of Chemistry, University of Illinois at Chicago, 845 W. Taylor St. (m/c111), Chicago, Illinois 60607-7061

Received: July 1, 2010; Revised Manuscript Received: August 20, 2010

Unordered proteins, unfolded peptides, and several "random coil" models have been shown to have local conformations similar to that of polyproline II (PPII). Inter-residue coupling of selected residues in a series of related peptides having predominantly PPII conformations were measured using IR, VCD, and Raman spectra of selected variants that were doubly C_1-labeled with ^{13}C on the amide C═O. The characteristics of the ^{13}C═O component of the IR, VCD, and Raman amide I′ bands and their sensitivity to the local structure of the peptide are compared to predictions based on DFT level calculations for related structures and used to estimate coupling interactions between pairs of C═O groups along the backbone of this helical structure. In the PPII case, the coupling is relatively weak, due to the extended structure, yet by combining IR, Raman, and VCD observations with results of DFT level model calculations, we have determined bounds for experimental interaction constants for this structure. Correlation of properties for PPII structures with those of "random coils" can be done by comparing Pro_n and Pro-rich sequences with Lys-rich sequences. The experimental band shifts and implied couplings reflect the computed results in both cases. Thermal unfolding of these peptides appears to be multistate, with monotonic spectral changes but little evidence of a cooperative (sigmoidal) transition. For the Lys-rich series, a transition from PPII to α-helix structure was induced by TFE addition, and the spectra were fit to an equilibrium model. These spectral changes show a large variation in ^{13}C═O coupling that occurs with a local conformational change from PPII- to α-helical, which is both well-fit by our theoretical results and offers a new site-specific method of assigning local PPII/disordered vs α-helical (or other) structure.

Introduction

Protein secondary structure is often categorized in terms of helices, sheets, and coils, with the latter category being ill-defined and containing all those components that do not fit well into the two dominant repeating forms. The nature of the "coil" has been a topic of interest for some time now. As originally suggested by Tiffany and Krimm and later demonstrated by a number of different studies, many "random coil" peptides and denatured proteins can, in large part, be shown to contain local left-handed turn character, commonly called the polyproline II helix (PPII).[1−4] The presence of these conformations is quite independent of proline content, and they are characterized by a broad energy minimum whose stability results, at least in part, from directing the amide C═O group out from the helix axis so that hydrogen bonds to the solvent are facilitated. Thus, the stability of such PPII conformers is quite solvent dependent for shorter peptides.

Studying the conformation of disordered proteins and peptides is particularly challenging because those techniques normally used for atomically resolved structure determination, such as X-ray and NMR methods, are dependent on the molecules having uniform structure, precisely what such disordered systems lack. Optical spectra, due to their very fast sampling of the molecular structure, can reflect the dynamic fluctuations of such structures, but usually cannot yield site-specific information. Normally, only average secondary structure components can be determined, and these are subject to both experimental and modeling errors. The key to spectral determination of structure is the coupling of repeating components in the sequence and its impact on the spectrum. Spectral patterns in electronic circular dichroism (ECD) are due to coupling of amide electronic ($\pi-\pi^*$) excitations, and those in vibrational CD (VCD) and spectral shifts in IR (infrared) and Raman spectra (particularly for the amide I′, C═O stretch) are similarly due to the coupling between amide vibrations.[5−9] For vibrational transitions, this coupling can be termed the off-diagonal part of the force field (FF). While the diagonal FF shifts with external perturbations such as hydrogen bonding, most of those effects are similar for different secondary structure types, making the diagonal effects less structure discriminating. However, those diagonal shifts have little impact on the coupling between amides, which in turn are highly dependent on the stereochemistry of the polymer backbone.

IR is a powerful technique for sensing the peptide secondary structure, but due to its resolution limitations only average backbone conformational data can normally be determined. However, if combined with isotopic labeling, IR gains sensitivity to site-specific structural aspects of the peptide through vibrational coupling of selected residues. The spectra of the labeled modes can be modeled using quantum mechanical (QM) force fields and atomic polar tensors (APT) for frequencies and intensities, respectively, as well as with empirical methods, as has been demonstrated by a number of applications.[10−22] Similarly, Raman spectra can provide alternate spectral patterns that may expose couplings with a different emphasis.[23−25] In addition, the associated VCD spectra of these peptides provide

* To whom correspondence should be addressed. E-mail: tak@uic.edu. Fax: (312) 996-0431.

10.1021/jp106095q © 2010 American Chemical Society
Published on Web 09/10/2010

TABLE 1: Sequences and Labeling Pattern of Peptides Used in This Study

notation	length/label position	sequence[a]
P14U	14/none	PPPPPPPPPPPPPP-NH_2
P14T	14/P7P8	PPPPPPP*P*PPPPPP-NH_2
P14A	14/P6P8	PPPPPP*PP*PPPPPP-NH_2
A14U	14/none	WPPPPAAAAPPPPK-NH_2
A14T	14/A7A8	WPPPPAA*A*APPPPK-NH_2
A14A	14/A6A8	WPPPPA*AA*APPPPK-NH_2
K14U	14/none	KKKKKAAAKKKKWK-NH_2
K14T	14/A6A7	KKKKKA*A*AKKKKWK-NH_2
K14A	14/A6A8	KKKKKA*AA*KKKKWK-NH_2

[a] Starred residues denote ^{13}C labeled on the amide C═O.

added resolution and a sign characteristic dependent on the conformation for the same isotope-shifted components. These spectra can all be further compared to theoretical models. That brings out conformational variations in spectral response. As we previously showed for various isotopic substitution patterns in α-helical peptides, by use of VCD in combination with IR one can sometimes resolve component bands that overlap significantly (when the splitting is less than the bandwidth).[26] Such a resolution can also be sometimes obtained by combining IR and Raman spectra due to the differences in their intensity mechanisms (which is particularly true for cross-coupled strands). This potential is dependent on conformation, so coupling such studies with theoretical analyses is a vital and important aspect of such a study.

Thermal unfolding of small peptides is usually less cooperative than found for single-domain proteins. The resulting thermal denaturation curves are often characterized by very broad transitions.[27,28] In this paper, we present data for isotope-labeled model PPII helices containing both Pro-based and Lys-based sequences (as denoted in Table 1) and show that the coupling constants and spectral patterns reflect our theoretical simulations. To isolate specific site-dependent FF couplings, the peptides are ^{13}C double labeled on the amide C═O either on two sequential positions (together, T) or on two positions separated by one unlabeled residue (apart, A), which lie in the center of a relatively long (14-residue) peptide to ensure uniform structure. Theoretical models provide the expected signs and magnitudes of the coupling interactions, and the experimentally identified shifts, although small, confirm the validity of the computed signs and relative intensity distributions. Consequently, the comparisons with experimental spectral shifts are used to provide upper and lower bounds to the interaction magnitudes. Equilibrium studies are then presented to model relative stabilities of the PPII helix form with regard to temperature and solvent variation. The latter highlights the unique coupling interactions in terms of both sign and magnitude for the PPII and α-helices, allowing their local discrimination.

Experimental Section

General Aspects. Materials and reagents purchased were of highest commercially available grade and used without further purification. ^{13}C labeled Fmoc-alanine and Fmoc-proline were purchased from Cambridge Isotope Laboratories, Cambridge, MA. Peptides were synthesized in house on a 0.1 mmol scale by standard solid-phase methods on Rink amide resin. In this process, 5 equiv of amino acids were activated with HBTU, HOBt (final concentration of 0.25 M), and DIEA at a final concentration of 0.5 M. A stepwise coupling of each amino acid was obtained using standard Fmoc coupling chemistry. Once the synthesis was complete, the peptide was removed from the resin using a cleavage cocktail (by dissolving in 95:2.5:2.5 TFA/water/EDT for 2 h). Crude peptides were isolated by precipitation into 10 volumes of cold ether, purified by reverse-phase HPLC (Vydac 218TP510 reversed-phase column on Waters 600 system), and characterized by ESI-MS (Thermo LTQ-FT LC/MS/MS). For IR and VCD spectral measurements, the peptides were deuterium exchanged, and TFA was removed by lyophilization of the peptide from a deuterated hydrochloric acid solution at pH* = 1.

Spectral Measurements. Mid-IR absorption spectra were measured as an average of 1024 scans at 4 cm^{-1} resolution using a Digilab FTS-60A FTIR spectrometer with a DTGS detector. Peptides were dissolved in deuterated phosphate buffer (pH* = 6.8) at ~40 mg/mL for both IR and VCD measurements, and some samples were also dissolved in TFE for solvent-induced conformational variation tests. Solution samples were placed in a home-made demountable cell constructed using a 50 μm Teflon spacer sandwiched between CaF_2 windows and sealed with a brass ring. The same samples were utilized for both IR and VCD spectra measurements.

VCD spectra were measured using a new homemade dispersive instrument with high S/N in the amide I and II region based on a 0.3 m (Acton) monochromator with a C-rod source and narrow band-pass, cooled MCT detector, which has been described separately.[29] Peptide VCD spectra with good S/N were typically obtained as an average of 8 repeated scans at 12 cm^{-1} spectral resolution over the amide I′ region of 1760−1540 cm^{-1}. Baselines were normally obtained under identical conditions by measuring VCD of a separate cell containing only buffer, and the result was subtracted from the sample spectrum as a correction.

All Raman measurements were carried out with a higher peptide concentration, ~100 mg/mL in D_2O, to minimize interference from the water bending mode at ~1650 cm^{-1}. Good S/N was obtained after 6 h of acquisition for each peptide at this concentration. The Raman spectrometer utilized a 90° collection geometry with excitation at 785 nm (380 mW, Innovative Photonic Solutions) which passed through a quartz cuvette containing 150 μL of sample solution. A planoconvex lens (f/1) placed one focal length from the cuvette was used to collect the scattered light. The elastic (Rayleigh) component was rejected by an edge filter (Semrock) before entering a lens (Nikon Nikkor 50 mm f/1.2) that focused the scattered light onto the slit of a Jobin-Yvon HR640 monochromator equipped with a CCD detector (Newton, Andor Technology). Known Raman transitions of cyclohexane and of a mixture of acetonitrile/toluene (50/50 volume solution) were fit to a second-order polynomial equation to develop a wavenumber calibration curve for the detector output. The baselines were corrected by subtracting a straight line in the amide I′ region.

For CD experiments, peptide solutions were prepared at approximately 0.2 mg/mL in 20 mM phosphate buffer pH = 6.8 and, alternately, in a series of TFE/H_2O mixtures. Far-UV CD spectra were acquired between 185 and 250 at 50 nm/min, with a 1 nm bandwidth and 2 s response time on a Jasco J-810 spectrometer using a 1 mm quartz cell (Starna, Inc.). Determination of sample concentration was based on absorbance at 280 nm (Trp $\varepsilon = 5560\ M^{-1}\ cm^{-1}$) for the K14 series and A14 series of peptides (for sequences, see Table 1), or by weighing and dilution for the P14 series. Final spectra were recorded as an average of eight scans and baseline subtracted. Variable-temperature experiments were done with a 1 °C/min ramp speed and a 5 min equilibration time, the temperature being controlled by flow from a water bath (Neslab RTE7DP). Spectra were

obtained over the range of 5−85 °C (in steps of 5 °C) for sample and buffer (for baseline subtraction) under identical experimental conditions.

Computational Details. Quantum mechanical IR spectral simulations were performed using density functional theory (DFT) methods on model PPII peptide structures. The first model was constructed as a relatively small (pentapeptide) Ala oligomer in vacuum whose backbone torsions were constrained to (φ, Ψ) = (−78°, +145°), appropriate for the PPII conformation. These smaller oligomer results provided APT and atomic axial tensors (AAT), for simulating IR and VCD intensities, respectively, as well as polarizability derivatives for Raman, which could be transferred along with the FF to longer peptides that were constructed to have the same secondary structures. The Bour Cartesian tensor transfer method is now well established.[12,15] It uses representations of the atomic contributions to the FF, etc., tensors of the small molecule and, by appropriate correction for tensor orientation, applies (transfers) them to construction of a new FF and intensity representation for the larger molecule that contains all local interactions but neglects long-range couplings. The resulting FF and APT matrices for IR, AAT for VCD, and polarizability derivatives for Raman were transferred to our programs for spectral simulation and isotopic substitution.[12] These diagonalize the transferred FF to give vibrational mode frequencies and apply the corresponding normal mode vectors to the intensity parameters to yield the simulated IR, Raman, and VCD spectra, as we normally represent them.[15]

To investigate effects of the sequence variations used experimentally, several other calculations were made by inserting selected Pro residues in the test sequence selected for comparison simulations of the isotope-labeled models with Ala-Pro mixed sequences. Finally, full DFT computations with correction for solvation using the COSMO variant of PCM[30] were made for a Pro_7 peptide constrained in a PPII conformation to determine any impact of transfer (end effects) and side chain, and the parameters were transferred to a Pro_{13} model. Isotope effects were computed by changing the appropriate atomic masses (^{12}C to ^{13}C on C_1=O, plus H to D where exchangeable) after parameter transfer and before diagonalization of the FF to get frequencies and intensities for comparison to experimental patterns.

Computations were done at the 6-31G*/BPW91 level using Gaussian 03 on a Linux-based machine with four 64-bit processors and shared memory (16GB).[31] The BPW91 functional is faster than the conventionally used hybrid functional (B3LYP) and for the amide I and II (where relevant) gives better frequency results, as we have previously shown.[14] Band-shape analyses of the simulated and experimental spectra, using second derivative and Gaussian component fitting, used both GRAMS and Origin software packages. The parameters were adjusted to minimize the contribution of noise to the fits and optimize the number of components, enhancing their interpretability.

Results

Peptide Design. The sequences and related isotope labeling schemes for three groups of 14-mer peptides which were investigated in this study are listed in Table 1. All these 14-mers are blocked at the C-termini by an amine group, yielding a terminal primary amide, and their N-termini were left unprotected. Each group of three peptides forms a series including the unlabeled sequence, denoted as U (unlabeled), one labeled sequentially with ^{13}C on the amide C=O's at the residue 7 and 8 positions (6 and 7 for the K14T), denoted as T (labeled "together") and another one labeled alternatively at the residue 6 and 8 positions, denoted as A (labeled one "apart"). The P14 series are proline oligomers designed to yield a stable PPII conformer as a standard for comparison, in which P14T has two sequential ^{13}C labels, and P14A has two labeled amides separated by one unlabeled residue.[3] The A14 series is meant to provide the same conformation with a more heterogeneous sequence, in that it is proline-rich but has four alanines in the middle flanked by four prolines on each side. The tryptophan and lysine residues are introduced for concentration determination and to enhance solubility, respectively, yielding a 14-residue peptide. The K14 series is a lysine-rich sequence, normally viewed as a model for random coils, but with three alanines at the A6, A7, and A8 positions and a tryptophan for concentration determination. Locating the ^{13}C labels on alanine amide C=O's in the A14 and K14 series was chosen to balance conformational integrity with expense.

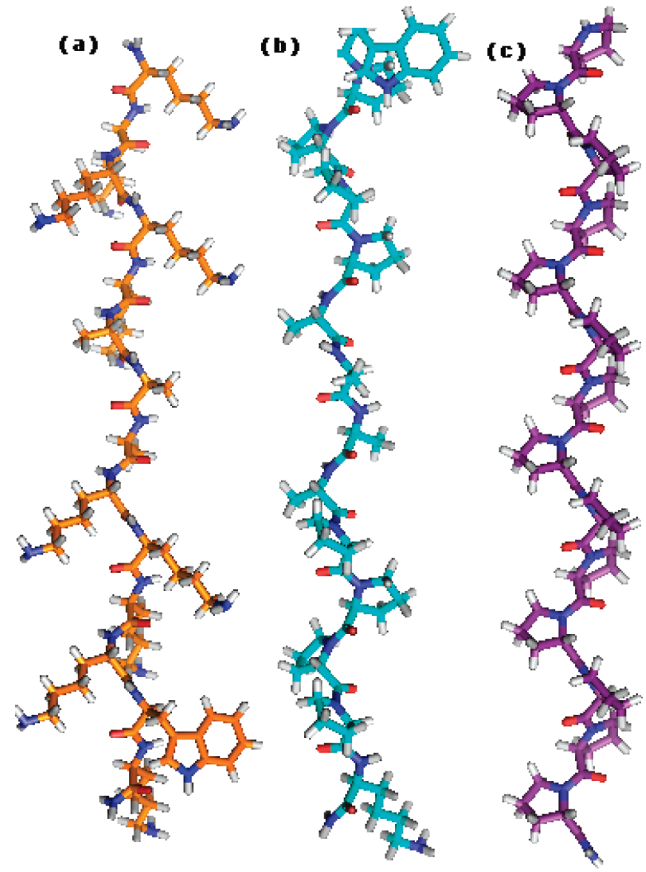

Figure 1. Structural models of (a) K14U, (b) A14U, and (c) P14U restricted to polyproline II conformation.

Idealized structures for the P14, A14, and K14 sequences are illustrated in Figure 1, a, b, and c, respectively. Conformational characterization of these peptides was first investigated by UV-CD, as shown in Figure 2. Spectra of unlabeled sequences are presented here, since the isotope-labeled ones have spectra identical to the unlabeled ones. The P14U, A14U, and K14U spectra share common features, having negative maxima at ∼195−205 nm and positive maxima at ∼210−220 nm which are typical of a PPII helix.[5] The wavelength shift of the peak positions is correlated to the number of Pro residues in the different sequences. Since the P14 series has exclusively tertiary amides (no N−H), the P14U yields UV-CD minima/maxima at the longest wavelengths (lowest energy). By contrast, the K14 series has all secondary amides, which results in the CD spectrum of K14U appearing at the shortest wavelengths (highest

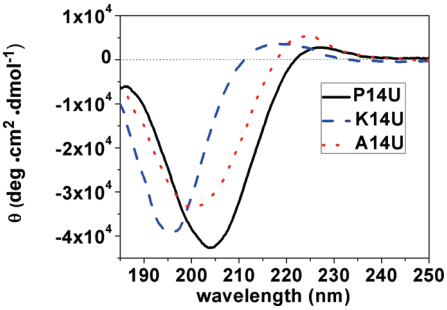

Figure 2. CD spectra of P14U, A14U, and K14U (P14U, black solid line; K14U, blue dashed line; A14U, red dotted line) in phosphate buffer pH = 6.83, collected at 5 °C.

energy). A14U contains a mixture of secondary and tertiary amides, and its CD lies between those of P14U and K14U. However, perhaps surprisingly, the A14U spectra are not broader than the P14U CD, even though they evidence effects of mixing two amide types. The band shape, which is dependent on stereochemically sensitive coupling of the amide transitions, independent of their frequencies, is the same for all these peptides, thus indicating that the peptides all have a common structural basis.

In principle, the concentration-corrected CD signal intensity, expressed as $[\theta]$ (molar ellipticity per residue), could be used to estimate the fractional structural content of these peptides. If we take $[\theta]$ at the characteristic minimum of P14U to be an intensity calibration for a maximally formed 14-mer PPII helix (which is not 100% but is as close as would be reasonable for a modest length, high-temperature sample), and compare that to the $[\theta]$ values at the negative maxima for K14U and A14U, we would conclude that their PPII contents were high, >80%.[32] Even taking into account the errors in concentration determination and the inherent approximations in such a comparison, we can conclude that there is very large fraction of PPII helical conformation in each of these peptide sequences.

Simulated Vibrational Spectra of Idealized PPII Structures. As noted earlier, theoretical modeling of the coupling of isotope-labeled bands and of their intensity distribution is an important tool for interpreting the spectral data we obtain. In Figure 3a,d,g, simulated amide I′ IR, VCD, and Raman spectra are compared for an Ac-P_{13}-$NHCH_3$ peptide constrained to the PPII conformation. These computed spectra are not corrected for the typical DFT FF error (which is mostly due to lack of correction for H-bonding solvent),[17,18,33] and hence the ^{12}C-amide I′ frequencies are too high (~60 cm^{-1} in this case with PCM solvent correction, but ~100 cm^{-1} for the Ala_{22} model in vacuum; Figure S1, Supporting Information). These can be contrasted with computed spectra for the isotope substituted variants, which have two ^{13}C═O-labeled groups placed both sequentially (T, dash line) and alternately (A, dotted line), in the center of the sequences. In the amide I′ IR spectra, Figure 3a, the computed ^{12}C band at ~1685 cm^{-1} loses intensity upon ^{13}C substitution, and the resulting ^{13}C band appears as a shoulder at ~1640 cm^{-1}. Below these spectra, expansions of the ^{13}C═O band are shown in Figure 3b,e,h (T) and Figure 3c,f,I (A) for the IR, VCD, and Raman, respectively, to emphasize the contributions of the coupled labeled modes. Comparable dipole strengths (D) are computed for each split ^{13}C component, which represent the in-phase and out-of-phase modes, in P14T and the corresponding components are only weakly split in P14A. Consequently, the sequentially and alternatively labeled peptides are predicted to have equivalent apparent IR spectral band shapes.

While the dipole intensity distribution suggests that T should have a slightly lower frequency mode than A as expanded in Figure 3, b and c, respectively, for realistic bandwidths this may not be detectable. For two labels together, the splitting between the ^{13}C modes is predicted to be 6 cm^{-1}, indicating the coupling between them should be ~3 cm^{-1} with the lower frequency mode having a higher intensity, which should shift the apparent ^{13}C band down from the average of the two modes. By contrast, the high-frequency mode in the A case is more intense but is barely separated (~1 cm^{-1}) from the low-frequency one, resulting in an overall band position close to that of the unperturbed ^{13}C mode. As indicated by the dash traces in Figure 3, b and c, if we fit the summed band shapes to a single Gaussian component, as done for the experimental spectral analyses, the ^{13}C band will appear at 1642 cm^{-1} for the T isomer and 1643 cm^{-1} for the A isomer. The 1 cm^{-1} difference between these two fitted bands would be less than the coupling between the two modes in T isomer and suggests that fitting the IR would only provide a lower bound to the coupling constant.

Although the VCD spectra computed for the same amide I′ transitions naturally has the same component mode positions as the IR, a very different intensity distribution is obtained for the two labeling schemes due to the signed nature of VCD bands. As shown in Figure 3d, when the components are plotted with a realistic band shape and summed, the VCD still results in a single (negative) shoulder on the dominant negative band. Due to the sign change, fitting a single Gaussian to the ^{13}C component for VCD results in a band at ~1640 cm^{-1} for T and ~1647 cm^{-1} for A. The difference, 7 cm^{-1}, is greater than the coupling constant and suggests that the VCD might provide an upper bound. Taken together, fitting the experimental VCD and IR ^{13}C band components may provide a means of extracting a range of values for the underlying coupling in the T (sequential labeling) case.

Raman modeling was done in a similar manner, and the ^{13}C═O amide I′ components are predicted to have the opposite relative intensity patterns as for IR. Consequently, our simulated Raman ^{13}C amide I′ shoulder profiles are about the same as the IR ones for A, with small splitting and a component predicted at ~1643 cm^{-1} but for T are shifted up to ~1644 cm^{-1} and again would yield a lower bound (1 cm^{-1}) to the coupling. However, if these patterns are impacted by variations in the sequence, particularly in the tertiary vs secondary amide shifts of the diagonal FF or by added aromatic residues having significant side-chain contributions which are common in Raman, this would be difficult to resolve.

To investigate impact of Pro residues on the theoretical modeling, we investigated a number of mixed structures. That most relevant one is the Ala_5-based calculation which is constrained to the PPII geometry. When propagated onto A_{22}, this yielded a pattern fully compatible with that discussed above for P14 except the coupling was somewhat larger. These computational results are summarized in Figure S1 of the Supporting Information.

Experimental Vibrational Spectra. *P14 Series.* Experimental IR, VCD, and Raman spectra for the amide I band in the three peptides forming the P14 series are shown in Figure 4, a, b, and c, respectively. In P14A and P14T, a weak broadened sideband is evident on the low-frequency side of the main amide I for each spectral technique. However, the sidebands for these three measures of the amide I each have different frequencies which are most evident for the P14T series. This pattern directly

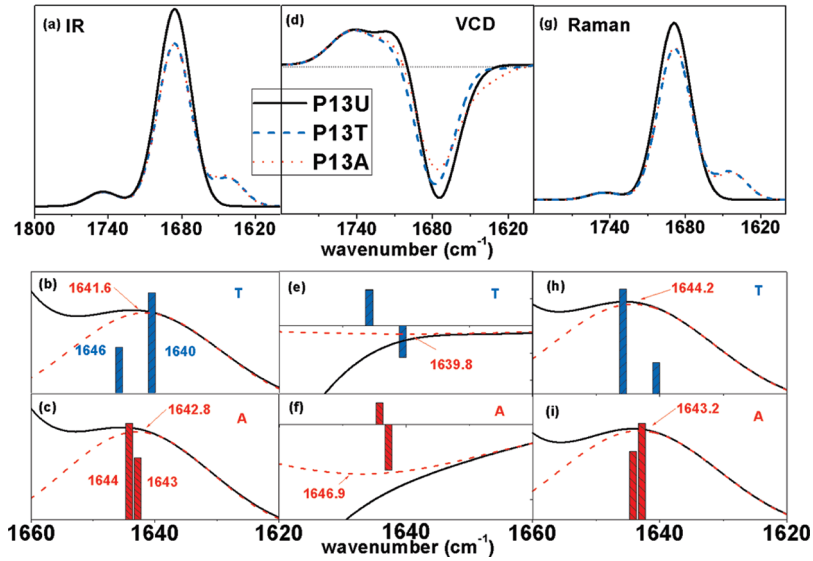

Figure 3. Simulated amide I′ FTIR (a), VCD (d), and Raman (g) spectra for the unlabeled Ac-P_{13}-NH_2 (black solid line), compared to the sequential (blue dashed line) and alternate (red dotted line) doubly labeled ones adopting polyproline II conformation. Panels (b) and (c) are simulated ^{13}C amide I′ IR spectra and normal mode contributions for T (sequential labels) and A (alternate labels). Panels (e) and (f) are simulated ^{13}C amide I′ VCD spectra and normal-mode contributions for T and A. Panels (h) and (i) are simulated ^{13}C amide I′ Raman spectra and normal-mode contributions for T and A. The coupling of the two $^{13}C{=}O$'s is interpreted to be half the splitting of the ^{13}C modes.

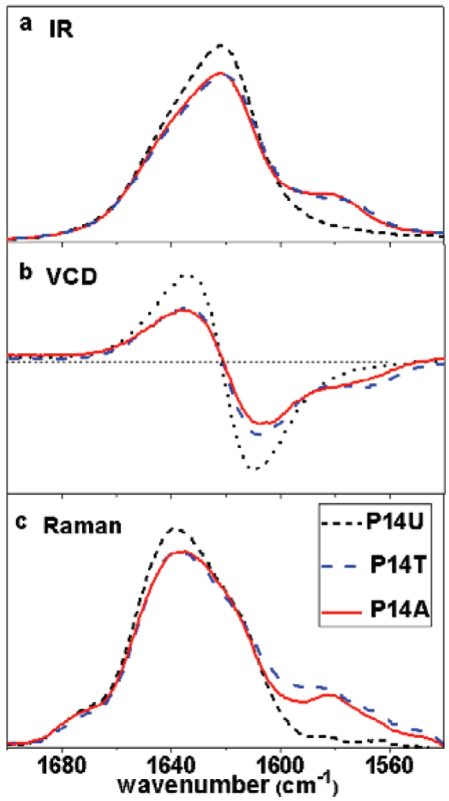

Figure 4. Experimental IR (a), VCD spectra (b), and Raman spectra (c) of P14 series of peptides (P14U, black short dashed line; P14T, blue dashed line; P14A, red solid line) in d-phosphate buffer pH* = 7 at 25 °C.

follows the predictions above; i.e., the main ^{13}C intensity is higher in frequency for Raman and lower for VCD than for IR spectra.

The quite small spectral difference between the T and A isomers seen for the experimental band shapes in the ^{13}C region still evidence a uniform pattern that the IR absorbance maximum and (negative) VCD for the ^{13}C sideband has a slightly lower frequency for the T isomer than for the A isomer. In Figure 4a, experimental IR spectra of the P14 series are overlaid and compared with similar presentations of the VCD and Raman spectra of the same set of peptides in Figure 4, b and c. Use of such overlapped spectra enhances the differences in the relative A and T ^{13}C shifts from the ^{12}C band. The unlabeled P14U (black solid line) shows a single maximum at 1620 cm^{-1} with an unresolved shoulder to high frequency in its amide I′ IR spectrum, in good agreement with a typical IR spectrum of poly-L-proline in the PPII helical conformation.[3] Upon isotope labeling, the intensity of the ^{12}C band decreases, and a ^{13}C band appears at around 1580 cm^{-1} with the band for T (blue dashed line) slightly lower in frequency than for A (red dotted line). The difference in the ^{13}C positions has a small impact on the overall band shape but it can be resolved with second derivatives (see below).

VCD spectra confirmed that these P14 peptides maintain a predominantly PPII secondary structure, since all exhibit a negative maximum at ~1610 cm^{-1} and positive maximum at ~1635 cm^{-1} for the ^{12}C region. In addition, the ^{13}C region in the VCD has a clearer frequency/intensity difference between the T and A isomers than was seen in the IR, with the T ^{13}C component being lower in frequency than the A, as predicted from the computed VCD−IR comparison above.

Overlaid Raman spectra of P14 series in Figure 4c are also consistent with the structure being PPII dominant helix in that the amide I′ maximum for P14U occurs at higher wavenumbers than in the IR and has a shoulder to low (rather than high) frequency. The isotope-shifted ^{13}C shoulder bands further validate the predictions from theory, showing a higher frequency for the T isomer than for the A isomer, although this is very difficult to resolve, being evidenced by higher intensity in the gap between the ^{12}C and ^{13}C bands for P14T.

The arguments above are all based on comparative inspection of the overlaid band shapes and a comparison of their consistency in terms of relative band shifts with that predicted above by our theoretical modeling. An alternate approach to finding band frequencies is to compute the second-derivative representation of the amide I spectra and from that determine the positions of the negative maxima (for IR and Raman) to

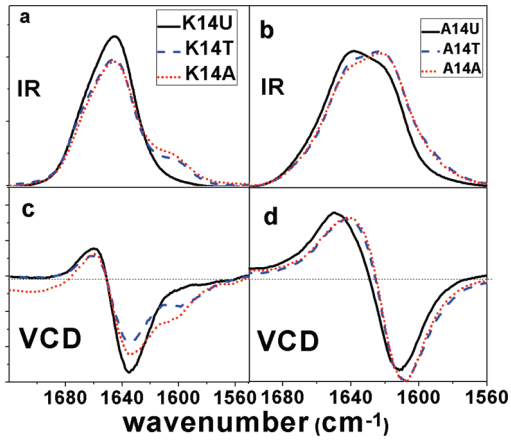

Figure 5. Experimental IR (a,b) and VCD spectra (c,d) of K14 and A14 series of peptides (U, black solid line; T, blue dashed line; A, red dotted line) in d-phosphate buffer pH* = 7 at 25 °C, respectively.

yield the band positions. The results for the P14 (and other series) are included in Table S1 (Supporting Information) and show the same consistency with the predicted pattern of shifts for the $^{13}C{=}O$ band as discussed above. However, the magnitudes are not necessarily what would be expected. In contrast to the very small shifts seen in the overall band profile and predicted theoretically, the second derivative gave 5 cm^{-1} difference from P14T (1573 cm^{-1}) to P14A (1578 cm^{-1}), while the apparent VCD difference was only 3 cm^{-1} (1567 and 1570 cm^{-1}, respectively). This deviation from the visual impression of the band-shape comparison and the prediction of our model is a bit surprising and suggests that perhaps the second-derivative model may have a weakness. Second derivative analyses of the Raman data were not very useful due to their higher noise level. The results are sensitive to the parameters chosen (27 points were used), and the P14A result evidenced a split band (1567 and 1574 cm^{-1}). As an alternate method, we undertook a band-fitting analysis, as presented in the Discussion.

K14 Series. IR and VCD spectra of the K14 series peptides are shown in Figure 5, a and c, respectively. These spectra resemble the P14 series results except that the ^{12}C amide I′ maximum IR absorbance appears at 1640 cm^{-1}, a behavior consistent with the K14 peptides having only secondary amides which have higher amide I′ frequencies than do the tertiary amide bonds in the P14 series.[3] In both the IR and VCD of the K14 series, the ^{13}C sideband occurs at a higher frequency for the A than for the T isomer, although this again is difficult to see in the overlapped shoulder but does become more apparent with second derivatives as well as band fitting (see Discussion). The consistency of the K14 results with the PPII predictions further confirms that the conformational nature of these unordered or "random coil" peptides is very similar to that of the PPII structure. The second-derivative results for the $^{13}C{=}O$ band give the same separation, 4 cm^{-1}, for the K14T and K14A IR and VCD bands, but the IR frequencies (1600 and 1604 cm^{-1}, respectively) are uniformly higher than the VCD values (1597 and 1601 cm^{-1}, respectively), as shown in Table S1 (Supporting Information). This shift presumably results from the near-equivalent dipole strengths of the in-phase and out-of-phase components in IR as contrasted with the large difference in their rotational strengths in the VCD, which would favor the lower frequency, negative ^{13}C component in VCD, as found in our computations (see Figure S1, Supporting Information). Corresponding Raman spectra of these peptides have an interfering band from the Trp residue that obscures the contribution from the ^{13}C labels, so those data are not shown.

A14 Series. The vibrational spectra of the A14 series, which have a mix of secondary and tertiary amides, are much more complicated, particularly with regard to ^{13}C labeling. In contrast to the one characteristic ^{12}C amide peak as in the case of P14U or K14U, the A14U ^{12}C amide I′ IR spectrum has two major bands that arise from the different characteristic frequencies for secondary (Xxx-Ala) and tertiary amides (Xxx-Pro), respectively, with a higher intensity maximum at 1640 cm^{-1}(secondary) and a lower maximum at 1620 cm^{-1}(tertiary). As shown in Figure 5b,d, the IR and VCD spectra of the two labeled isomers do not show a distinguishable ^{13}C band, but both labeled peptides have IR and VCD profiles that are shifted down in wavenumber from the A14U spectrum and evidence a shift of intensity from the higher to lower wavenumber band consistent with a contribution to the intensity from ^{13}C on secondary amide bonds. When two alanines are ^{13}C substituted, part of the higher frequency secondary amide component is shifted down, leading to higher intensity for the lower frequency component in both of A14T and A14A. However, due to the lower energy tertiary amide component, the ^{13}C band is not resolved as either a sideband or shoulder. The same problem affects the VCD spectra of the A14 series, shifting the entire spectrum down due to overlap of the ^{13}C features with the tertiary amide VCD. Despite these complications, even this mixed structure shows spectral patterns that are qualitatively consistent with the theoretical predictions, although quantitative deconvolution is probably not possible.

Discussion

General Aspects. We have synthesized and studied PPII peptides designed as either all Pro or partial Pro containing or "random coil" models but each exhibiting fully consistent CD and VCD which demonstrates they have an underlying PPII structure.[2,3,5,34] Theoretical (DFT) modeling of the IR and VCD shows a consistent pattern for peptides labeled on adjacent (T) positions to have a lower frequency $^{13}C{=}O$ band than those labeled on alternate (A) positions in the sequence. The opposite is true for the Raman. These predictions were qualitatively borne out in the spectra obtained for all three series of peptides we prepared, P14, K14, and A14, but the spectral differences between the two labeling patterns were small. Second-derivative analysis showed the experimental $^{13}C{=}O$ features to have the correct relative frequency pattern, but the magnitudes varied from theoretical expectations, and such an analysis was not feasible for the A14 series due to spectral overlap. Further band-shape analysis was aided by band-fitting enabled deconvolution, as described below, which yielded similarly correct relative patterns and more interpretable magnitudes. The lack of resolution of the exciton split components in the experimental spectra is perhaps best modeled by fitting with a constrained number of components to match the heterogeneous broadening. Thus, we have established and demonstrated a distinct pattern for isotopic labeling effects on the IR, VCD, and Raman intensity and frequency distributions. The next step in such an analysis would be to establish a quantitative correlation between theoretical prediction and experimental results.

Coupling Constant Estimation. To more quantitatively determine the positions of the ^{13}C band contributions to the vibrational spectra of all the 14-mers studied, multicomponent band fittings of the IR, VCD, and Raman spectra were performed, and the results are shown in Figure 6 for the P14 series (analyses for K14 series and A14 series are shown in the Supporting Information, Figures S2 and S3, and detailed parameters of the fits are summarized in Table S1). Initial band

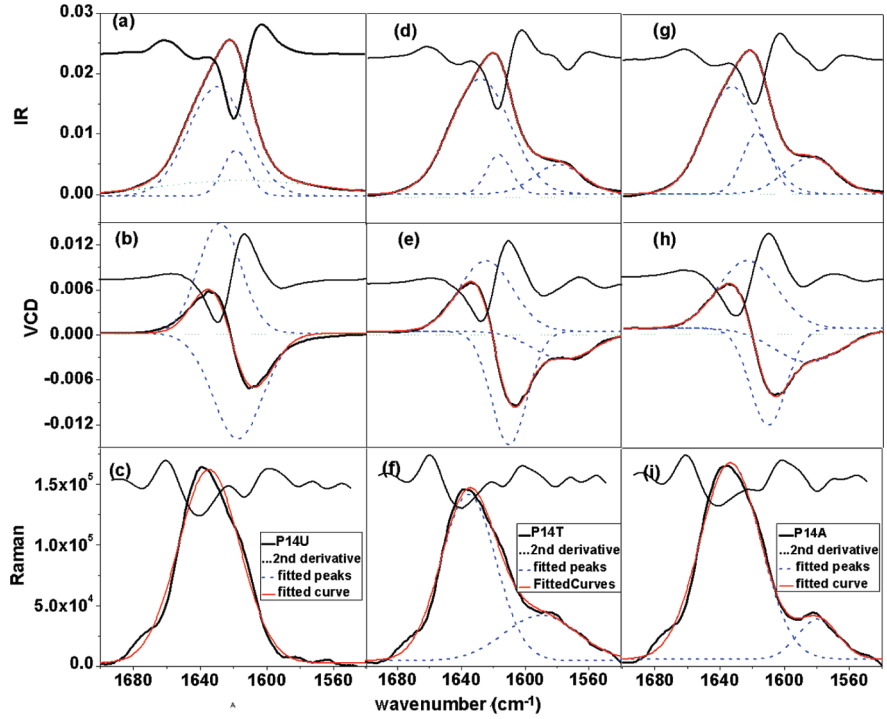

Figure 6. Experimental IR, VCD, Raman, their second-derivative spectra (above), and multiple Gaussian peak fitting profiles (overlaid, dashes) of P14 series of peptides (black traces are original spectra, red traces are overall fitted curves, short dotted lines are second-derivative spectra, dashed lines correspond to the fitted Gaussian functions): (a) IR of P14U, (b) VCD of P14U, (c) Raman of P14U, (d) IR of P14T, (e) VCD of P14T, (f) Raman of P14T, (g) IR of P14A, (h) VCD of P14A, and (i) Raman of P14A.

positions for each component were obtained from second derivatives, which indicated three major components for the labeled P14 and K14 components.[35−38] Fits to three Gaussian components, which were allowed to vary in central frequency, bandwidth, and area, led to good agreement with the experimental IR, as can be seen from the fitted overall traces. These fitted components are relatively broad, ranging from 15 to 34 cm^{-1}, implying a heterogeneous broadening or lack of resolution of underlying components as would be expected for a moderate length oligopeptide with a partially fluctuating structure. In principle, the relative areas of these peaks should correspond to the relative magnitudes of the dipole strengths of the assigned component modes, if the coupling between $^{13}C{=}O$ and $^{12}C{=}O$ modes were minimal. This is approximately correct for the P14 and K14 series IR, as can be seen from the normalized areas listed in Table S1 (Supporting Information) but is not as useful for VCD due to the need to add a very broad weak component for baseline correction.

The magnitude of the $^{13}C-^{12}C$ shift observed in these fits is consistent with our calculations and is of the order of 35−40 cm^{-1}. The fitted ^{13}C band for P14T has a central frequency of 1579 cm^{-1} and normalized area of 0.16, and the corresponding values for P14A are 1585 cm^{-1} and 0.20. The difference of 6 cm^{-1} should correspond to a lower limit of coupling constant of P14T, assuming (1) that the splitting of the two ^{13}C components for P14A is very small, as we have calculated, and (2) that the lower wavenumber $^{13}C{=}O$ component has the higher intensity of the pair (see Figure 3). If we had relied upon second derivatives alone, the lower limit would be suggested to be 5 cm^{-1}, in reasonable agreement, even though the center frequencies are different, with the second derivatives being 6−7 cm^{-1} lower. The intensity ratio for 2 residues out of 14 should be ∼0.14, so both $^{13}C{=}O$ bands are close to the expected intensity value (probably within error) but may evidence some intensity borrowing from $^{12}C{=}O$ modes. The similarly fit areas (13.7%) derived from our simulated P14T and P14A spectra precisely match the ideal expectation.

The VCD was also fit with a sum of three Gaussian bands but in this case with one positive and two negative components for the labeled P14T and P14A. The $^{13}C{=}O$ frequency difference of the A and T variants derived from the VCD fit is larger than from the IR fits, which would be expected given the oppositely signed rotational strengths predicted for the in-phase and out-of-phase modes. Fitting this to just one negative band will make the A−T difference an upper bound for the coupling in P14T $^{13}C{=}O$ modes, assuming the P14A modes are unresolved. The fitted VCD ^{13}C band for P14T has a central frequency of 1576 cm^{-1} and the corresponding value for P14A is 1586 cm^{-1}. This larger difference of 10 cm^{-1} from the band fitting suggests an upper bound for the P14T coupling constant; however, in this case the second-derivative result yields a smaller difference, 3 cm^{-1}, which suggests some error in either method. Inspection of the data and fits shows the P14A VCD $^{13}C{=}O$ spectral component to be broader than seen for any of the other fits and the second derivative to result in two maxima, which averaged gave the 1570 cm^{-1} value in the table. Smaller upper bound values for the P14T coupling would then be consistent with the K14 results and with the simulations. The values obtained for the experimental upper and lower bounds of the P14T interaction are both higher than predicted theoretically from the fitted calculated spectra in Figure 3, where it demonstrates the coupling of the two ^{13}C modes in T isomer is 3 cm^{-1} and corresponding difference in IR ^{13}C bands as 1 cm^{-1} while that in VCD is 7 cm^{-1}.

The same fitting strategy was used for all the IR, Raman and VCD spectra of the P14, K14 and A14 series and a summary of the ^{13}C band information extracted from the fits is in Table 2. Details of these other fits are provided in Figures S2 and S3 as well as in Table S1 of the Supporting Information. The K14 ^{13}C bands have essentially the same pattern but some quantitative

TABLE 2: Coupling Constants Derived from ^{13}C Amide I′ Peak Positions of Labeled Peptides from Band-Shape Fitting Results

	^{13}C fitted peak position (cm^{-1})		
notation	IR	VCD	coupling const (cm^{-1})
P14T	1579	1576	6−10
P14A	1585	1586	
K14T	1609	1600	3
K14A	1612	1603	
A14T - A14U	1599	1598	6[a]
A14A - A14U	1605	1604	

[a] Overlapping bands make this determination have high error.

differences. The $^{13}C-^{12}C$ splitting is 28−32 cm^{-1}, smaller than that for P14, and the difference in the K14T and K14A ^{13}C band positions in both IR and VCD is only 3 cm^{-1}, again smaller than P14. The K14 band areas are consistent with those of P14. This lack of frequency shift suggests that the local modes in K14 are actually higher in frequency than the observed ^{12}C maximum. This may be due to a Lys (charged) side chain effect on the local (residue specific) FF, leading to the dominant ^{12}C═O maximum in K14, as compared to the neutral and small Ala side chain, which is on the labeled residues. We have seen shifts, although smaller in magnitude, between Lys and Ala in model peptide calculations (Lakhani et al., unpublished results).

To analyze the A14 series spectra, difference spectra (A14T−A14U, A14A−A14U) were obtained to help identify the spectral variations in more detail (Figure S3, g and h, Supporting Information).[39] The negative minima in the IR difference spectra (Figure S3) correspond to the ^{12}C band loss and the positive maxima to the ^{13}C gain. Despite the smaller separation compared with that in the fitted Gaussian peaks, these difference spectra show the same trends in peak positions for the isotope-substituted variants as calculated in our idealized models. For VCD, the differences are more complex due to the signed nature of the spectrum, but the ^{13}C component (low-frequency band) shows a negative difference contribution, which is a gain of negative VCD as would be predicted for ^{13}C in a PPII helix. That the A14A has more negative intensity than does the A14T isomer is again consistent with our theoretical result. Despite the complications of overlapping bands, even in the A14 series the qualitative theoretical patterns based on oppositely signed coupling in A14A and A14T come through in the analysis of the experimental data.

Derivation of coupling constants could be done by correlating experimental results and simulated ones, and our best estimates are listed in Table 2. Since resolution of components remains an issue, we must assume that the A coupling is small, <1 cm^{-1}. The band-fitting results then yield coupling constants for the T isomer in the range of 6−10 cm^{-1} in the P14 series, 3 cm^{-1} in the K14 and 6 cm^{-1} (from the fits) in the A14 series, while the second derivatives suggest a smaller value for the P14 series (3−5 cm^{-1}) more in agreement with the K14 result.

Thermodynamic Stability of the K14 Series of Peptides. Thermal denaturation experiments using CD and IR spectroscopies were conducted for all the peptides in the current study over the range of 5−85 °C (see Supporting Information, Figure S4, for thermal variation spectra). However, when intensity variations vs temperature were plotted, only gradual, roughly linear changes were observed with no sign of cooperative unfolding. Presumably the 3_1-helical core in these peptides gradually changes in length as temperature is increased but the final (φ, Ψ) angles in the disordered peptides still sample the general area of Ramachandran space that lies near those (φ, Ψ) angles associated with the PPII conformation. The high thermal stability of the PPII helical conformation, along with the similarity of spectral response between the folded and unfolded state, inhibits the utility of studying this unfolding transition upon simple thermal perturbation.[40,41] Therefore, we resorted to variation of solvent conditions to change the stability of the PPII helix with respect to α-helix for the K14 peptide series.

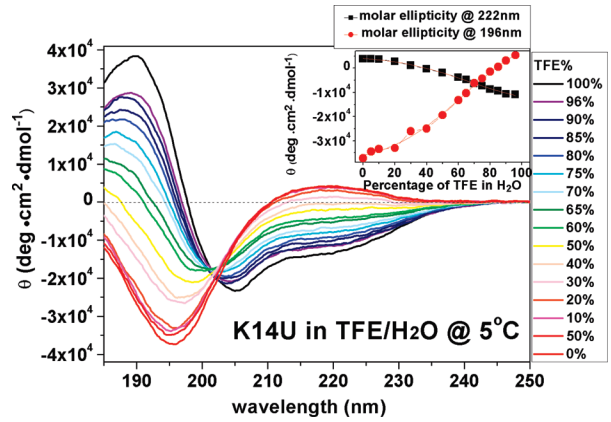

Figure 7. CD spectra of K14U in mixtures of water and TFE at 5 °C, TFE% ranged from 0% (pure water) to 100%. Inset: plotted CD signal at 222 nm (■) and 196 nm (●) against the fraction of TFE in water.

The PPII helix is the dominant conformation for K14 in water, whereas an α-helical conformation is favored for many sequences (without Pro) in solvents such as TFE.[42−44] Switching the PPII to α-helix by addition of TFE to the water solvent depends on the relative conformational stability of the two helical forms in each environment. It would be impossible for the P14 series peptide to form an α-helix since its (φ, Ψ) space is restricted by formation of the cyclic Pro side chain and the all-Pro sequence cannot form the intrachain H-bonds necessary to stabilize the α-helix against solvation. These issues, in turn, favor formation of the PPII or 3_1-helical conformation in water since its amide C═O groups are directed out toward the solvent permitting stabilization via H-bonding. Consequently, we chose the K14 series to study the solvent-induced conformational transition, since it can support both helical forms.

By titrating K14U in different mixtures of TFE and water at 5 °C, as shown in Figure 7, the CD pattern becomes inverted from coillike (PPII) to partial helical (α) as the TFE concentration is increased. Monitoring molar ellipticity at 222 nm yields a transition curve changing from positive to negative values with increasing TFE fraction, while molar ellipticity at 196 nm changes more dramatically from negative to positive values, as expected for loss of the PPII conformation. The spectral changes representing the two conformations vary in a like (anticorrelated) manner. The inset in Figure 7 shows the variation in molar ellipticities at these two characteristic wavelengths vs TFE fraction in water, and fitting these data to a function representing an equilibrium transition suggests that the turnover from PPII to α-helix occurs at ∼65% TFE in H_2O. The final (100% TFE) state is still only partially α-helical (∼48%, as estimated using CDPro,[45,46] a value which will be somewhat uncertain due to the solvent change). The mixed nature of the final state is also evident from the shape of the CD in the 200−230 nm range. In these terms, a complete coil to helix transition is not seen here, nor could it be.

Isotope-edited IR spectra can provide a very sensitive probe of local secondary structural changes in peptides, as we have previously indicated in the thermal melting studies of Ala-rich

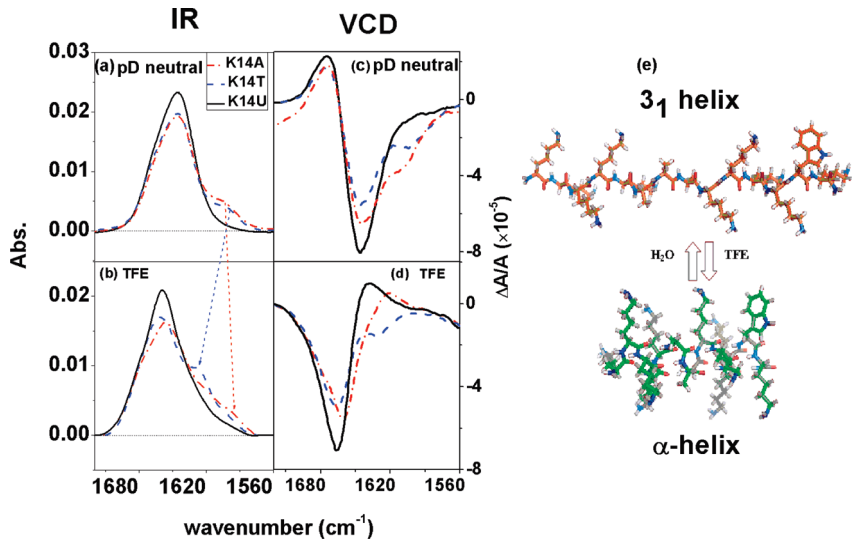

Figure 8. IR and VCD spectra of K14 series of peptides (K14U, black solid line; K14T, blue dashed line; K14A, red dotted line) in d-phosphate buffer pH* = 7 (a, c) and in TFE (b, d). (e) Molecular model illustration of K14U in different solvents, modeled as the polyproline II conformation in D_2O and α-helical conformation in TFE.

α-helical peptides as well as selected β-hairpin model peptides.[11,47,48] Labeling can also help develop an understanding of these solvent-induced PPII to α-helix transitions. Shown in Figure 8a−d are comparisons of the amide I′ IR and VCD for the K14 series of peptides in deuterated phosphate buffer and in TFE. In pure TFE where the peptides adopt a predominantly α-helical conformation, IR spectra are in qualitative agreement with the results of our previous study on alanine-rich peptides with the same labeling schemes.[26] Converting from PPII helix in aqueous condition to α-helix in TFE, the ^{12}C bands shift up ~10 cm^{-1} for K14U and more dramatic effects are evident in the ^{13}C features. The trends computed and observed above, in which K14T in a PPII structure has a lower $^{13}C{=}O$ frequency than K14A, is not only reversed for the α-helical form, but a much larger frequency difference between the K14A and K14T results, offering a clear resolution of A and T substitution patterns for the α-helix conformation (TFE) as indicated by dashed arrows in Figure 8.

The larger separation occurs because of both larger coupling interactions and the opposite intensity patterns for the two substitution patterns in the α-helix, which yield a difference in the observed $^{13}C{=}O$ position that is roughly a lower bound to the sum of the two larger coupling constants. By contrast, as noted before, the PPII structure has much weaker coupling and the difference in peak position corresponds to a lower bound of just the sequential coupling constant. It might not be obvious why coupling falls off in the 3_1-helical geometry. This is effectively an extended chain, differing form the fully extended (flat β-strand) by a 120° vs 180° twist. The C=O groups are spread further apart in the 3_1-helix and the angle between dipoles further reduces the dipole coupling as compared to the more parallel case for α-helices. The resulting characteristic coil to α-helix isotope band shifting detectable in just the IR can serve as direct evidence of the structural transition suggested by the model in Figure 8e. The sign reversal of the sequential $^{13}C{=}O$ coupling constant is precisely what was predicted with these and earlier DFT computations of the force field and subsequent simulations of the effects of ^{13}C labeling on the IR and VCD. The shift of the labeled residues is diagnostic of local structural change, and by extension from our previous studies, is not limited to discriminating disordered from α-helical structures.[10,26,47,48] Such data provide graphic evidence of how the site-specific coupling of amides observed in vibrational spectra can be diagnostic of site-specific secondary structure.

Conclusions

Experimental results and theoretical simulations demonstrate that coupling between sequential amide C=O's in a PPII helical structure can be identified using isotope-edited vibrational spectroscopy with specific ^{13}C labeling schemes. Using 14-residue proline oligomers as an ideal PPII helix model, with sequential and alternate ^{13}C labels on two central amide C=O's, the sequential (i, $i + 1$) coupling constant was estimated to be in the range of 6−10 cm^{-1} from band fitting, and probably lower, 3−5 cm^{-1}, from second-derivative analyses, while the coupling between alternate (i, $i + 2$) C=O's was too weak to be evaluated, and those with larger separations (i, $i + 3$, etc.) were not attempted. This method could be extrapolated to explain the interaction in other peptide sequences that adopt a PPII conformation such as proline-rich or lysine-rich sequences with ^{13}C labels on alanine amides. Though the actual values for the coupling constants derived from the observed IR and VCD spectra of these model systems may deviate from simulations, their orders of magnitude and signs are shown to be reliable and the resulting frequency pattern is fully consistent with theory. Such a conserved trend could be useful for other studies of structural transitions where the response of ^{13}C labels can be sensed, which should include coherent 2D IR studies. Dramatic changes in label frequencies were observed when TFE was used to induce a PPII to α-helical transition for lysine-rich sequences, suggesting its use as a new local structure diagnostic. These findings have extended the use of isotope-labeling vibrational spectroscopies to investigate various secondary structures of peptides, particularly for PPII helices of interest in disordered peptides and proteins.

Abbreviations: APT, atomic polar tensor; CCD, charge-coupled device; DFT, density functional theory; DIEA, diisopropylethylamine; DTGS, deuterated triglycine sulfate; ECD, electronic circular dichroism; EDT, ethanedithiol; ESI-MS, electrospray ionization mass spectrometry; FF, force field; FMOC, fluorenylmethyloxycarbonyl; FT, Fourier transform; HBTU, *O*-benzotriazole-*N*,*N*,*N*′,*N*′-tetramethyluronium hexafluorophosphate; HOBt, *N*-hydroxybenzotriazole; HPLC, high-

performance liquid chromatography; IR, infrared; MCT, mercury cadmium telluride; PCM, polarized continuum model; pH*, measured pH value in D_2O solution; PPII, polyproline II; QM, quantum mechanical; S/N, signal-to-noise ratio; SVD, singular value decomposition; TFA, trifluoroacetic Acid; TFE, 2,2,2-trifluoroethanol; Tm, midpoint of thermal change profile; VCD, vibrational circular dichroism.

Acknowledgment. This work was supported by a grant for the National Science Foundation (CHE07-18543 to T.A.K.). We thank Petr Bour and Josef Kapitan for providing initial coordinates for the Pro-based calculations.

Supporting Information Available: Simulated spectra for Ala_{22} peptides in PPII conformation, and details of band fitting to experimental data as well as added thermal variation data. This material is available free of charge via the Internet at http://pubs.acs.org.

References and Notes

(1) Tiffany, M. L.; Krimm, S. *Biopolymers* **1968**, *6*, 1379.
(2) Woody, R. W. *Adv. Biophys. Chem.* **1992**, *2*, 37.
(3) Dukor, R. K.; Keiderling, T. A. *Biopolymers* **1991**, *31*, 1747.
(4) Shi, Z. S.; Woody, R. W.; Kallenbach, N. R. *Adv. Protein Chem.* **2002**, *62*, 163.
(5) Woody, R. W. *J. Am. Chem. Soc.* **2009**, *131*, 8234.
(6) Keiderling, T. A.; Silva, R. A. G. D. In *Synthesis of Peptides and Peptidomimetics*; Goodman, M., Ed.; Georg Thieme Verlag: Stuttgart, Germany, 2002; Vol. E22b, p 715.
(7) Mantsch, H. H.; Chapman, D. *Infrared Spectroscopy of Biomolecules*; Wiley-Liss: Chichester, UK, 1996.
(8) Kubelka, J.; Bour, P.; Keiderling, T. A. In *Advances in Biomedical Spectroscopy*; Barth, A., Haris, P. I., Eds.; IOS Press: Amsterdam, 2009; Vol. 2, p 178.
(9) Hering, J. A.; Haris, P. I. In *Advances in Biomedical Spectroscopy*; Barth, A., Haris, P. I., Eds.; IOS Press: Amsterdam, 2009; Vol. 2, p 129.
(10) Kubelka, J.; Keiderling, T. A. *J. Am. Chem. Soc.* **2001**, *123*, 048.
(11) Silva, R. A. G. D.; Kubelka, J.; Decatur, S. M.; Bour, P.; Keiderling, T. A. *Proc. Natl. Acad. Sci. U.S.A.* **2000**, *97*, 8318.
(12) Bour, P.; Sopkova, J.; Bednarova, L.; Malon, P.; Keiderling, T. A. *J. Comput. Chem.* **1997**, *18*, 646.
(13) Bour, P.; Kubelka, J.; Keiderling, T. A. *Biopolymers* **2000**, *53*, 380.
(14) Kubelka, J.; Silva, R. A. G. D.; Keiderling, T. A. *J. Am. Chem. Soc.* **2002**, *124*, 5325.
(15) Kubelka, J.; Silva, R. A. G. D.; Bour, P.; Decatur, S. M.; Keiderling, T. A. In *Chirality: Physical Chemistry*; Hicks, J. M., Ed.; ACS Symposium Series; American Chemical Society: Washington, DC, 2002; Vol. 810, p 50.
(16) Hilario, J.; Kubelka, J.; Keiderling, T. A. *J. Am. Chem. Soc.* **2003**, *125*, 7562.
(17) Kubelka, J.; Huang, R.; Keiderling, T. A. *J. Phys. Chem. B* **2005**, *109*, 8231.
(18) Bour, P.; Keiderling, T. A. *J. Phys. Chem. B* **2005**, *109*, 5348.
(19) Kim, J.; Kapitan, J.; Lakhani, A.; Bour, P.; Keiderling, T. A. *Theor. Chem. Acc.* **2008**, *119*, 81.
(20) Kim, J.; Huang, R.; Kubelka, J.; Bouř, P.; Keiderling, T. A. *J. Phys. Chem. B* **2006**, *110*, 23590.
(21) Kim, J.; Keiderling, T. A. *J. Phys. Chem. B* **2010**, *114*, 8494.
(22) Bour, P.; Keiderling, T. A. *J. Phys. Chem. B* **2005**, *109*, 23687.
(23) Schweitzer-Stenner, R.; Measey, T.; Hagarman, A. *AIP Conf. Proc.* **2008**, *1075*, 18.
(24) Schweitzer-Stenner, R. *J. Phys, Chem. B* **2009**, *113*, 2922.
(25) Ahmed, Z.; Myshakina, N. S.; Asher, S. A. *J. Phys, Chem. B* **2009**, *113*, 11252.
(26) Huang, R.; Kubelka, J.; Barber-Armstrong, W.; Silva, R. A. G. D.; Decatur, S. M.; Keiderling, T. A. *J. Am. Chem. Soc.* **2004**, *126*, 2346.
(27) Brooks, C. L. *Acc. Chem. Res.* **2002**, *35*, 447.
(28) Karle, I. L. *Acc. Chem. Res.* **1999**, *32*, 693.
(29) Lakhani, A.; Malon, P.; Keiderling, T. A. *Appl. Spectrosc.* **2009**, *63*, 775.
(30) Klamt, A. COSMO and COSMO-RS. In *The Encyclopedia of Computational Chemistry*; Schleyer, P. R., Allinger, N. L., Clark, T., Gasteiger, J., Kollman, P. A., Schaefer III, H. F., Schreiner, P. R., Eds.; John Wiley & Sons: Chichester, UK, 1998; Vol. 1, p 604.
(31) Frisch, M. J.; Trucks, G. W.; Schlegel, H. B.; Scuseria, G. E.; Robb, M. A.; Cheeseman, J. R.; Montgomery, J. A.; Vreven, T.; Kudin, K. N.; Burant, J. C.; Millam, J. M.; Iyengar, S. S.; Tomasi, J.; Barone, V.; Mennucci, B.; Cossi, M.; Scalmani, G.; Rega, N.; Petersson, G. A.; Nakatsuji, H.; Hada, M.; Ehara, M.; Toyota, K.; Fukuda, R.; Hasegawa, J.; Ishida, M.; Nakajima, T.; Honda, Y.; Kitao, O.; Nakai, H.; Klene, M.; Li, X.; Knox, J. E.; Hratchian, H. P.; Cross, J. B.; Bakken, V.; Adamo, C.; Jaramillo, J.; Gomperts, R.; Stratmann, R. E.; Yazyev, O.; Austin, A. J.; Cammi, R.; Pomelli, C.; Ochterski, J. W.; Ayala, P. Y.; Morokuma, K.; Voth, G. A.; Salvador, P.; Dannenberg, J. J.; Zakrzewski, V. G.; Dapprich, S.; Daniels, A. D.; Strain, M. C.; Farkas, O.; Malick, D. K.; Rabuck, A. D.; Raghavachari, K.; Foresman, J. B.; Ortiz, J. V.; Cui, Q.; Baboul, A. G.; Clifford, S.; Cioslowski, J.; Stefanov, B. B.; Liu, G.; Liashenko, A.; Piskorz, P.; Komaromi, I.; Martin, R. L.; Fox, D. J.; Keith, T.; Al-Laham, M. A.; Peng, C. Y.; Nanayakkara, A.; Challacombe, M.; Gill, P. M. W.; Johnson, B.; Chen, W.; Wong, M. W.; Gonzalez, C.; Pople, J. A. *Gaussian 03*; Gaussian Inc.: Wallingford CT, 2004.
(32) Kelly, M. A.; Chellgren, B. W.; Rucker, A. L.; Troutman, J. M.; Fried, M. G.; Miller, A.-F.; Creamer, T. P. *Biochemistry* **2001**, *40*, 14376.
(33) Kubelka, J.; Keiderling, T. A. *J. Phys. Chem. A* **2001**, *105*, 10922.
(34) Krimm, S.; Bandekar, J. *Adv. Protein Chem.* **1986**, *38*, 181.
(35) Shanmugam, G.; Polavarapu, P. L. *J. Mol. Struct.* **2008**, *890*, 144.
(36) Moritz, R.; Fabian, H.; Hahn, U.; Diem, M.; Naumann, D. *J. Am. Chem. Soc.* **2002**, *124*, 6259.
(37) Oh, K.-I.; Han, J.; Lee, K.-K.; Hahn, S.; Han, H.; Cho, M. *J. Phys. Chem. A* **2006**, *110*, 13355.
(38) Cho, Y.; Sagle, L. B.; Iimura, S.; Zhang, Y.; Kherb, J.; Chilkoti, A.; Scholtz, J. M.; Cremer, P. S. *J. Am. Chem. Soc.* **2009**, *131*, 15188.
(39) Brewer, S. H.; Song, B.; Raleigh, D. P.; Dyer, R. B. *Biochemistry* **2007**, *46*, 3279.
(40) Kuemin, M.; Schweizer, S.; Ochsenfeld, C.; Wennemers, H. *J. Am. Chem. Soc.* **2009**, *131*, 15474.
(41) Decatur, S. M. *Biopolymers* **2000**, *54*, 180.
(42) MacPhee, C. E.; Perugini, M. A.; H. Sawyer, W.; Howlett, G. J. *FEBS Lett.* **1997**, *416*, 265.
(43) Bolin, K. A.; Pitkeathly, M.; Miranker, A.; Smith, L. J.; Dobson, C. M. *J. Mol. Biol.* **1996**, *261*, 443.
(44) Buck, M. *Q. Rev. Biophys.* **1998**, *31*, 297.
(45) Sreerama, N.; Woody, R. W. *Anal. Biochem.* **1993**, *209*, 32.
(46) Sreerama, N.; Woody, R. W. *Methods Enzymol.* **2004**, *383*, 318.
(47) Huang, R.; Setnička, V.; Etienne, M. A.; Kim, J.; Kubelka, J.; Hammer, R. P.; Keiderling, T. A. *J. Am. Chem. Soc.* **2007**, *129*, 13592.
(48) Huang, R.; Wu, L.; McElheny, D.; Bour, P.; Roy, A.; Keiderling, T. A. *J. Phys. Chem. B* **2009**, *113*, 5661.

JP106095Q